Characterization of nuclear-irradiated graphite by non-destructive beta spectrometry using a MLEM deconvolution algorithm

Lorenzo Fleres, Julien Venara, M Cuozzo, S Fargier, C Mahe, E El Haber, F Goutelard, Frédérick Carrel

Characterization of nuclear-irradiated graphite by non-destructive beta spectrometry using a MLEM deconvolution algorithm

L. Fleres [1*], J. Venara [1], M. Cuozzo [1], S. Fargier [1], C. Mahe [1], E. El Haber [1], F. Goutelard [2], F. Carrel [3]

[1] CEA, DES, ISEC, DPME, SEIP, LNPA, Univ. Montpellier, Marcoule, F-30207, Bagnols-sur-Cèze Cedex, France
[2] CEA, DES, DDSD, UARP, SIPS, GPRA, Marcoule, F-30207, Bagnols-sur-Cèze Cedex, France
[3] Université Paris-Saclay, CEA, List, F-91120, Palaiseau, France

[*]Corresponding Author, E-mail: lorenzo.fleres@cea.fr

KEYWORDS: Beta Spectrometry, Decommissioning, Deconvolution, Graphite, MLEM, 14C

Abstract

This study addresses challenges in characterizing nuclear-irradiated graphite from decommissioned reactors. Traditional liquid scintillation counting methods involve time-consuming steps for analyzing beta-emitting activation products. We propose a non-destructive method based on a plastic scintillation beta spectrometer coupled to a MLEM deconvolution algorithm. Using a MCNP6.2 numerical model of the detector, we obtained the reference datasets to perform the deconvolution of measured spectra on graphite samples. We determined the main activation products' activity values for both pure (^{14}C, ^{36}Cl, ^{90}Sr) and non-pure (^{60}Co, ^{133}Ba, ^{137}Cs, ^{152}Eu, ^{154}Eu) beta emitters. The proposed methodology would significantly reduce costs and time for measuring and characterizing irradiated graphite.

Graphical Abstract

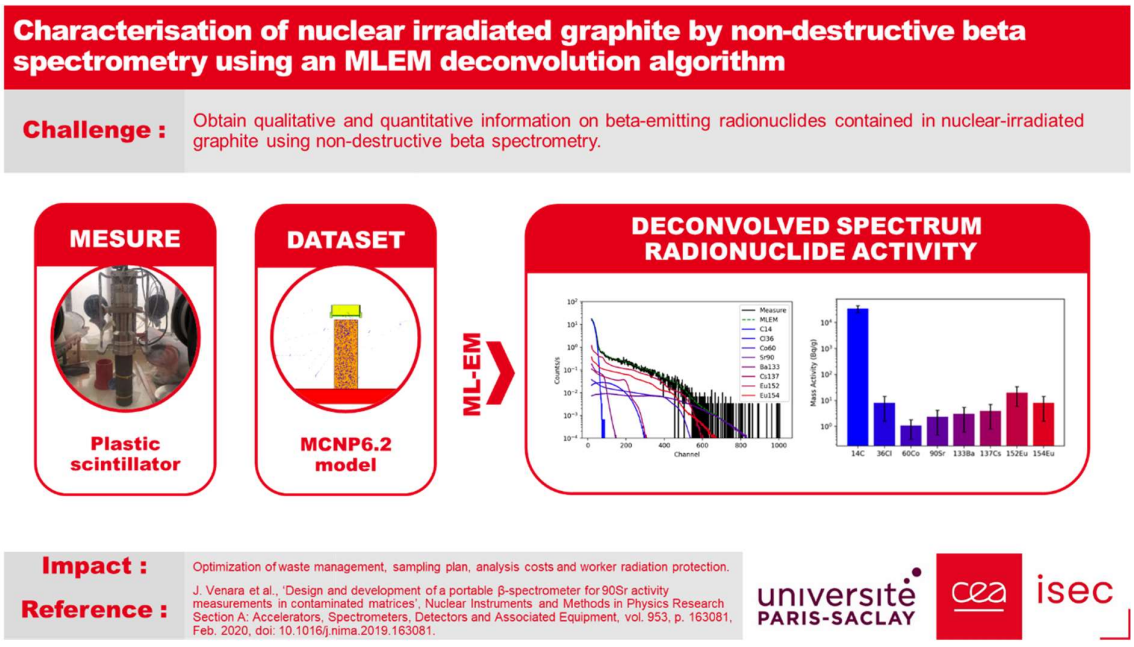

I. Introduction

The accumulation of approximately 250,000 tonnes of irradiated graphite worldwide represents a significant waste management challenge [1]. Graphite, utilized since the first nuclear reactor Chicago Pile 1 [2], has been integrated into the design of numerous nuclear plants due to its favorable chemical and physical characteristics, facilitating its role as a neutron reflector and moderator. The exposure of graphite to neutron flux induces physical alterations in its structure and leads to the generation of radionuclides, mainly through neutron activation. Out of them, irradiated graphite contains a large amount of long-lived radioisotopes, notably ^{14}C (with a half-life of approximately 5730 years) and ^{36}Cl (with a half-life of approximately 320,000 years). These radionuclide half-lives require careful consideration in waste disposal strategies, highlighting the importance of accurate characterization methods to guide safe storage practices. The pure beta-emitting nature of ^{14}C and ^{36}Cl complicates their detection and quantification using non-destructive methods. To date, these radionuclides are measured in laboratory conditions using liquid scintillation techniques [3-4]. While effective, the drawbacks of liquid scintillation counting methods include their destructive nature, high costs, time-intensive procedures, and the necessity for prior chemical operations [5]. There has been a growing interest in developing alternative non-destructive methodologies for characterizing pure beta emitters [6-11]. Such approaches offer the potential to obtain additional details while preserving sample integrity for future analyses. However, the continuous spectra generated by beta emissions pose an analytical challenge, necessitating deconvolution techniques to extract meaningful information. Several methodologies for the deconvolution of beta spectra have been developed in recent years [12-15], but they have yet to be applied to the characterization of nuclear graphite.

In this study, we present a new approach for non-destructive graphite characterization using a plastic beta spectrometer coupled with a Maximum Likelihood Expectation Maximization (MLEM) [16] algorithm. We tested the algorithm's performance to quantify the activities of beta emitters on spectra acquired on graphite samples from the G1 reactor located at the CEA Marcoule center.

The article is structured as follows. Section II presents the measurement setup and the characteristics of the graphite samples investigated. In section III, we introduce the deconvolution problem and describe the adopted methodology based on the MLEM algorithm. In section IV, we detail the generation of the response matrices using Monte Carlo simulations. Section V discusses the deconvolution results for fuel channel and reactor core samples. In Section VI, we state conclusions and perspectives for future works.

II: Measurement methodology and sample characteristics

CEA has developed a methodology based on a portable beta plastic scintillator spectrometer for *in situ* radiological characterization of ^{90}Sr in contaminated matrices [6]. The methodology requires two measurements: the first one with the bare detector and the second one with an aluminum cover placed over the detector. The cover was designed to stop the most energetic beta particles and to ensure that the detector only measures gamma rays. The subtraction of the two acquired spectra provides the beta component. The methodology was then extended to measure ^{14}C using an energy windowing approach [17]. Following the same measurement methodology, we acquired spectra of i-graphite samples retrieved during the investigation program of the Uranium Natural Graphite Gaz (UNGG) G1 reactor [18]. We analyzed the samples in a glove box, where we placed the beta spectrometer. The probe was connected using a LYNX multichannel analyzer (MIRION Technologies, CA, USA) to a computer equipped with the Genie 2000 software [19] for data acquisition and analysis.

A first set of 42 samples, about 20 mm long and 15 mm in diameter, were taken from core drills in 6 reactor fuel channels, as shown in Fig. 1a. For each sample, we analyzed the three faces: fuel channel side, graphite core side and longitudinal side. We set the distance of the detector from the working plane at 25 mm and the measurement time between 2 and 5 minutes, depending on the position of the sample in the reactor. The short measurement time was selected for the fast and accurate quantification of ^{14}C activity. Fig. 1b and Fig. 1c show the measurement setup and an example of the analyzed sample.

A second set of 15 samples, about 200 mm long and 67 mm in diameter, were obtained from the B2 core drill penetrating the reactor core vertically, as shown in Fig. 2a. Three out of the fifteen samples originated from the reflector graphite, the remaining twelve were retrieved from the moderator. The

larger sample size significantly increases the contribution of gamma-emitting radionuclides in the detector's response. The poorer beta signal to gamma noise ratio did not allow us to analyze the longitudinal faces of the samples. We analyzed each sample's two circular faces, corresponding to the top and bottom of a graphite brick. We set the distance of the detector from the top of the sample at 2 mm and the measurement time between 5 and 120 minutes, depending on the position of the sample in the reactor. The extended measurement time resulted in an increased counting statistic, thus improving the analysis of radionuclides other than ^{14}C. Fig. 2b and Fig. 2c show the measurement setup and an example of the analyzed sample.

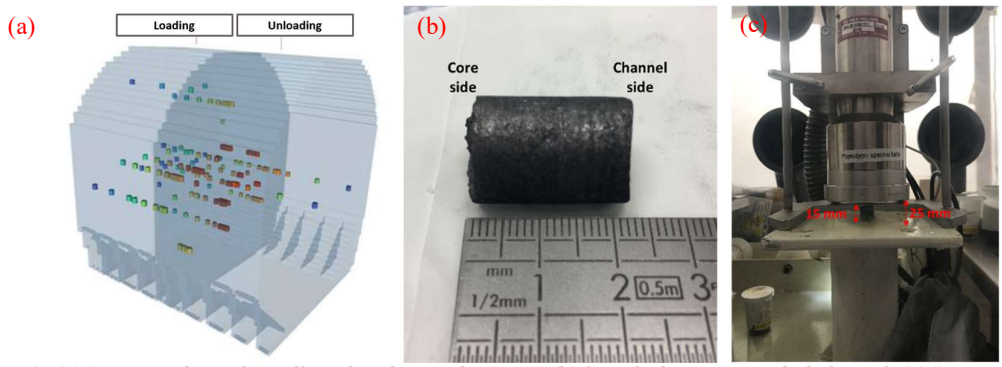

Figure 1: (a) Position of samples collected in the graphite core. (b) Sample from reactor fuel channel. (c) Beta spectrometry configuration.

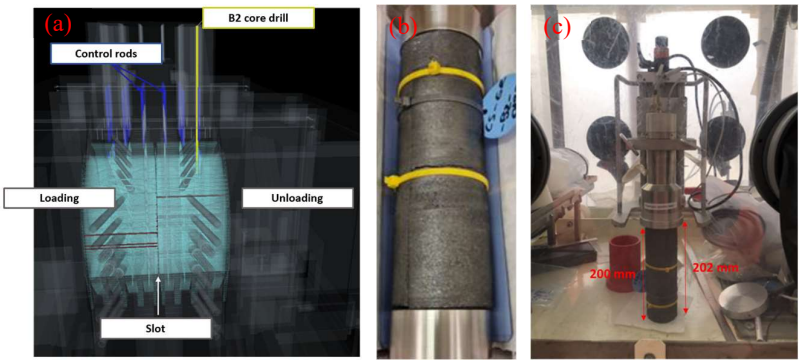

Figure 2: (a) Position of B2 core drill. (b) Sample from B2 core drill. (c) Beta spectrometry configuration.

III. Deconvolution problem and ML-EM algorithm

The deconvolution problem to be solved consists of quantifying the radionuclides present in a mixed source term. The relationship between the activity of different sources and the number of measured events in a spectrum can be expressed as follows:

$$\begin{bmatrix} Y_1 \\ Y_2 \\ \vdots \\ Y_C \end{bmatrix} = \begin{bmatrix} \varepsilon_{1,1} & \varepsilon_{1,2} & \cdots & \varepsilon_{1,S} \\ \varepsilon_{2,1} & \varepsilon_{2,2} & \dots & \varepsilon_{2,S} \\ \vdots & \vdots & \ddots & \vdots \\ \varepsilon_{C,1} & \varepsilon_{C,2} & \cdots & \varepsilon_{C,S} \end{bmatrix} \begin{bmatrix} \lambda_1 \\ \lambda_2 \\ \vdots \\ \lambda_S \end{bmatrix}$$

The $(C,1)$-dimensional vector Y corresponds to the acquired spectrum. The (C,S)-dimensional vector ε is the absolute efficiency matrix. The $(S,1)$-dimensional vector λ coincides with the number of particles emitted during the measurement. It is the unknown vector of the problem and is equal to the product $A \cdot I \cdot T$, where A is the activity of the source, I is the emission intensity, and T is the measurement time. Spectrum deconvolution problems aim to find a solution for the vector λ given the measured spectrum Y and the matrix ε. However, it is impossible to reconstruct the vector λ perfectly, as measurements and Monte Carlo simulations are subject to uncertainties that introduce statistical fluctuations. Commonly used methods to solve deconvolution problems are [20] Non-negative least squares (NNLS), Bayesian methods such as MCMC (Markov Chain Monte Carlo) and iterative methods such as the Maximum Likelihood Expectation Maximization algorithm. MLEM, without incorporating prior knowledge about

data probabilistic distributions, iteratively updates the estimated source emission vector until convergence. In particular, the goal of the MLEM method is to find an estimate $\hat{\lambda}$ of the vector λ, where $\hat{\lambda}$ is the vector that maximizes the probability of observing the measured spectrum Y given the matrix ε. The generic iteration of the MLEM algorithm is as follows [16]:

$$\hat{\lambda}_j^{[n+1]} = \frac{\hat{\lambda}_j^{[n]}}{\sum_i^C \varepsilon_{i,j}} \sum_i^C \frac{\varepsilon_{i,j} \cdot Y_i}{\sum_k^S \varepsilon_{i,k} \cdot \hat{\lambda}_k^{[n]}}$$

At iteration 0, an initial estimate of the vector $\hat{\lambda}$ must be defined and is usually set as the average of the initial values:

$$\hat{\lambda}_j^{[0]} = \frac{\sum_i^C Y_i}{\sum_i^C \sum_j^S \varepsilon_{i,j}}$$

Two major drawbacks of the MLEM algorithm are the absence of a precise stopping criterion for the iterations and the choice of the database size. To stop MLEM iterations, the user must define a stopping criterion. Generally, this is done by either setting a maximal number of iterations or by evaluating the absolute relative difference between $\hat{\lambda}_j^{[n+1]}$ and $\hat{\lambda}_j^{[n]}$, setting it to be lower than a defined value δ. The second major drawback of the algorithm is related to the size of the absolute efficiency matrix. The response matrix has *C* rows equal to the measured spectra channels and *S* columns equal to the number of sources. A certain number of *C1* and *C2* initial and final channels are usually excluded to eliminate measurement noise. The user defines the second dimension, *S*, selecting radionuclides likely to be present in the mixed source term. The results provided by the algorithm for the deconvolution of the same spectrum *Y* may vary according to the four parameters $(\delta, C1, C2, S)$. We applied the MLEM algorithm multiple times to the same measurement, changing *C1*, *C2* and δ parameters. This allowed us to gather statistical data on the deconvolution results. We maintained the number of sources *S* constant since all simulated radionuclides are expected to be present in our samples, as described in Section IV.

Examples of acquired spectra for the two sets of sample measurement configurations are shown in Fig. 3.

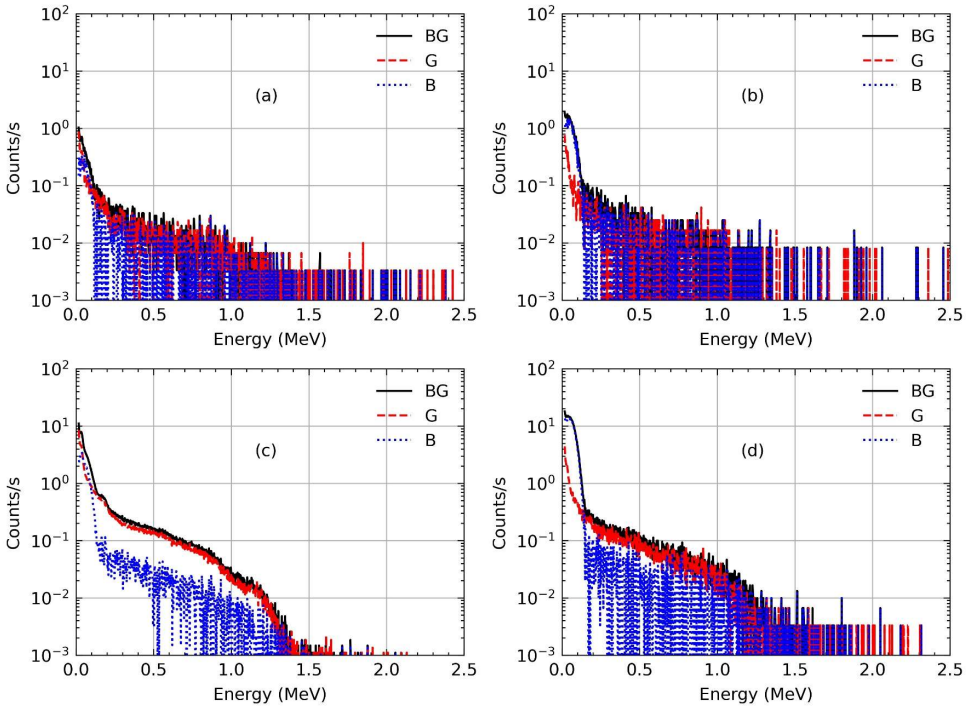

Figure 3: Measured beta+gamma (BG), gamma (G) and beta (B) spectra on different samples:
(a) Sample from channel 36-17C at 400 cm from the slot. Measurement time: 5 minutes.
(b) Sample from channel 36-17C at 30 cm from the slot. Measurement time: 3 minutes.
(c) Sample from B2 drill at 10 cm from the top of the reactor. Measurement time: 90 minutes.
(d) Sample from B2 drill at 310 cm from the top of the reactor. Measurement time: 5 minutes.

IV. Creation of response matrices by Monte Carlo simulations

The absolute efficiency response matrix ε must be determined to solve the inverse deconvolution problem. The matrix ε can be constructed using Monte Carlo simulations or reference spectra in the same measurement configurations. Since we did not dispose of such standard samples, we have modeled all measurement configurations using a numerical model. The MCNP6.2 detector model was qualified in laboratory conditions in previous works [6, 21]. This validation process revealed a good agreement between simulations and measurements, with a deviation of approximately 10% for a ^{14}C source. Fig. 4 illustrates the MCNP6.2 model used for the B2 sample measurement configuration.

Based on neutron activation calculations for the G1 reactor [22], we selected electron-emitting radionuclides with median activity exceeding 1 Bq g^{-1}. Table 1 summarizes the chosen radionuclides and their corresponding 5th, 50th, and 95th percentile activity values. We retrieved radioactive decay data from the JEFF3.3 library [23] for photons and discrete electron emissions. We used BetaShape [24] software to obtain beta emissions data, considering experimental shape factors. We assumed a uniform distribution in the sample since radionuclides are produced mainly by neutron activation in bulk graphite. This assumption likely holds for samples extracted from combustible channels, considering their small size. However, for larger-volume samples obtained from the B2 drill core, the validity of the homogeneous model becomes less certain. While it may serve as a starting point for our analysis, further investigation is necessary to assess the potential heterogeneity of radionuclide distribution in these larger samples. We evaluated the detector responses to the selected radionuclides using an *F8*-type tally in the plastic scintillator cell.

The beta and beta+gamma responses are shown in Fig. 5 for the measurement configuration of samples from the B2 core drill. Non-pure beta emitters exhibit a continuous gamma component due to the predominant Compton interaction of photons in the low-resolution plastic scintillation detector. The responses of ^{3}H ($E_{\beta,\,mean}$ = 6 keV, $E_{\beta,\,max}$ = 19 keV) and ^{63}Ni ($E_{\beta,\,mean}$ = 17keV, $E_{\beta,\,max}$ = 67 keV) are not shown since the mylar window stops the emitted electrons before entering the sensitive material. The proposed methodology is unsuitable for characterizing these two radionuclides; however, it enables the measurement of all other beta emitters, particularly ^{14}C and ^{36}Cl.

Radionuclide	$T_{½}$ (y)	Production Mode	Activity (Bq/g)			Emission
			PC5	PC50	PC95	
^{3}H	12.3	Neutron absorption of lithium	735.5	11041.5	28730.4	β
^{14}C	5730	Neutron activation from carbon and (n-p) reaction with nitrogen	1084.1	17026.1	55086.7	β
^{36}Cl	302000	Neutron activation from chlorine impurities	0.3	4.5	14.2	β
^{60}Co	5.3	Neutron activation from cobalt impurities	0.2	3.1	10.0	β, γ
^{63}Ni	98.7	Neutron activation from nickel impurities	11.0	170.1	542.6	β
^{90}Sr	28.8	Fission product from fissile impurities	0.3	4.8	22.3	β
^{133}Ba	10.5	Neutron activation from barium impurities	0.1	1.0	3.7	IC, X, γ
^{137}Cs	30.0	Fission product from fissile impurities	0.3	5.7	28.1	β, IC, X, γ
^{152}Eu	13.5	Neutron activation from europium impurities	0.1	14.2	42.1	β, IC, X, γ
^{154}Eu	8.6	Neutron activation from europium impurities	0.5	7.7	18.4	β, IC, X, γ

Table 1: Summary of the main electron-emitting radionuclides in the G1 reactor according to neutron activation calculations (referenced at date 2020). PC = percentile. IC = Internal Conversion electrons.

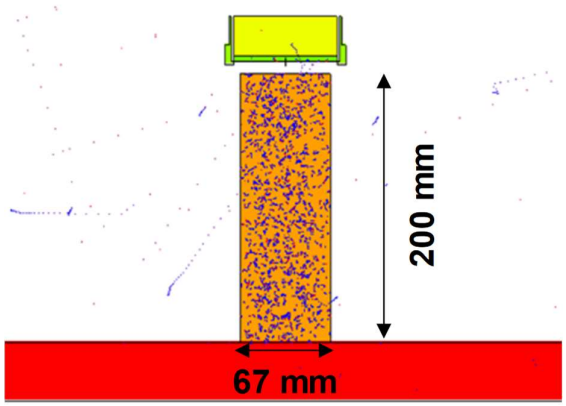

Figure 4: MCNP6.2 model of measurement configurations in the vertical position with graphite sample from B2 drill.

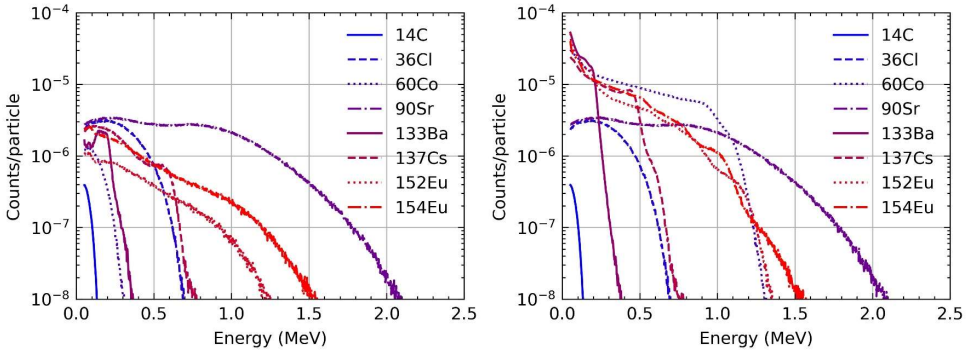

Figure 5: Beta and beta+gamma detector responses for main activation products with uniformly distributed activity (1 Bq) in the source volume.

V. Deconvolution results

V.I. Fuel channel samples

V.I.I. ^{14}C mass activity

We present results for samples collected from channels 20-18C, 21-17C and 36-17C. We applied MLEM deconvolution to the total beta+gamma and beta spectrum for each analyzed face. Given the more uniform surface of the longitudinal face compared to the circular faces of the samples, the mass activity determined from the horizontal measurement configuration should be considered the most representative value. Fig. 6 shows the ^{14}C mass activity evaluated using MLEM deconvolution and the energy window method [17].

^{14}C mass activity values obtained by the beta and beta+gamma MLEM deconvolution approaches are consistent, with a maximum relative deviation of less than 5 %. The successful beta+gamma deconvolution confirms the potential for eliminating the need for additional gamma measurements. This advancement translates to a significant reduction in overall measurement time (50%) and a simplification of the mechanical design and deployment. The relative deviations between the measured and calculated activity values are shown in Fig. 7. Out of the 18 samples analyzed, the estimated value exceeded the measurement uncertainty band in only two instances (31%, k=2). The total uncertainty is determined by considering Type A and Type B uncertainties. Type A uncertainty arises from the statistical fluctuations inherent in the measured count rate. Type B uncertainties encompass systematic effects, including the error observed between simulated and measured ^{14}C response and uncertainties associated with sample characteristics like size and density.

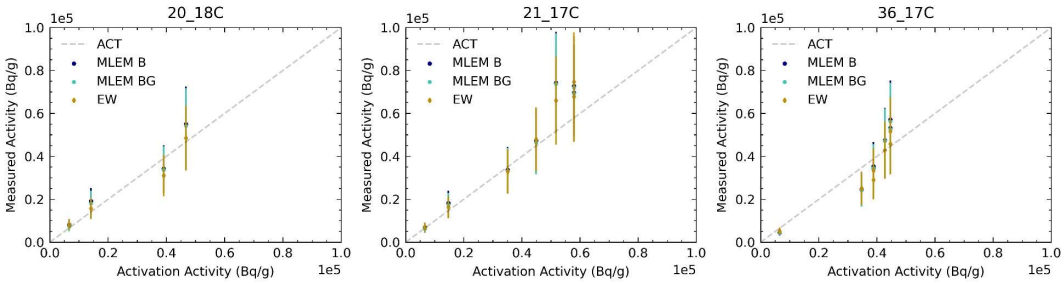

Figure 6:[14]C mass activity estimated using MLEM beta (B) deconvolution, MLEM beta+gamma (BG) deconvolution and energy window (EW) method for channels 20-18C, 21-17C and 36-17C samples.

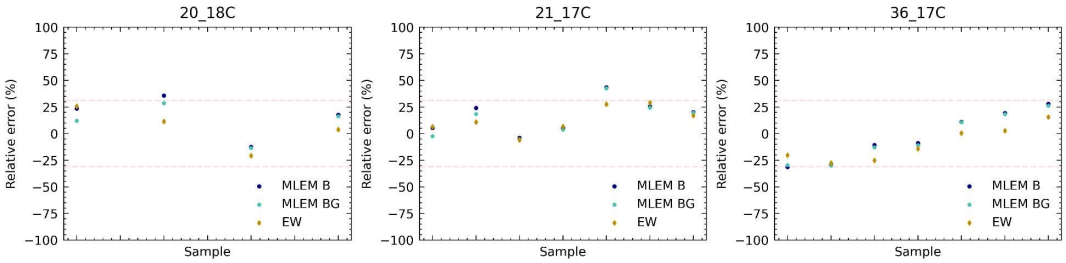

Figure 7: Relative deviations between measured and calculated [14]C mass activities for channels 20-18C, 21-17C and 36-17C samples. The red lines represent the measurement uncertainty band.

We discuss in more depth results for samples collected from channel 36-17C, as 5 out of 7 were also analyzed using liquid scintillation counting. Fig. 8 shows the ^{14}C mass activity evaluated for the three faces with different methods: non-destructive beta spectrometry using MLEM deconvolution and energy window (EW), liquid scintillation counting (LSC) and neutron activation calculation (ACT). ^{14}C mass activity values estimated by beta spectrometry on the longitudinal face gradually increase toward the center of the reactor from about 5000 to 60000 Bq/g, as summarized in Table 2. With an uncertainty of around 31% (k=2) on the measured mass activities, the calculated and measured values are globally consistent.

For samples obtained from the periphery of the graphite core (≤ 170 cm), the ^{14}C mass activities deduced from measurements on the three faces exhibit overall consistency within the uncertainty bounds. Comparison with neutron activation calculations shows an overestimation of the calculated activity. Analysis of additional samples will prove this overestimation, which is likely related to the uncertainty of the neutron flux profile in the outer core region. For samples collected at distances of 120, 60, 30, and 15 cm from the reactor center, ^{14}C mass activities on the channel face show an overestimation ranging from 40% to 70% compared to those derived from the longitudinal side. This phenomenon could arise from a higher ^{14}C production on the surface due to the ^{14}N (n,p) ^{14}C reaction occurring within nitrogen in the gas coolant. The overestimation may stem from an alpha contribution from the increased activation yield of minor actinides or surface contamination near the reactor slot. Alpha emitters could potentially noise the low-energy spectra region since the EJ200 exhibits a lower scintillation efficiency for alpha particles [25].

Position (cm)	MLEM (Bq/g)	EW (Bq/g)	LSC (Bq/g)	Neutron Activation (Bq/g)
400	$4.5x10^{03}$ (-31%)	$5.2x10^{03}$ (-20%)	No data	$6.5x10^{03}$
200	$2.5x10^{04}$ (-30%)	$2.5x10^{04}$ (-37%)	$2.2x10^{04}$ (-37%)	$3.5x10^{04}$
170	$3.4x10^{04}$ (-12%)	$2.9x10^{04}$ (-25%)	No data	$3.9x10^{04}$
120	$3.5x10^{04}$ (-10%)	$3.3x10^{04}$ (-14%)	$3.3x10^{04}$ (-16%)	$3.9x10^{04}$
60	$4.7x10^{04}$ (+11%)	$4.3x10^{04}$ (+0%)	$4.3x10^{04}$ (0%)	$4.3x10^{04}$
30	$5.3x10^{04}$ (+19%)	$4.6x10^{04}$ (+3%)	$4.4x10^{04}$ (-2%)	$4.5x10^{04}$
15	$5.7x10^{04}$ (+27%)	$5.1x10^{04}$ (+16%)	$4.7x10^{04}$ (-5%)	$4.5x10^{04}$

Table 2: Comparison of [14]C mass activities for 36-17C channel samples. Relative deviation from the activation calculations value in brackets. MLEM values represent the mean between beta and beta+gamma deconvolution.

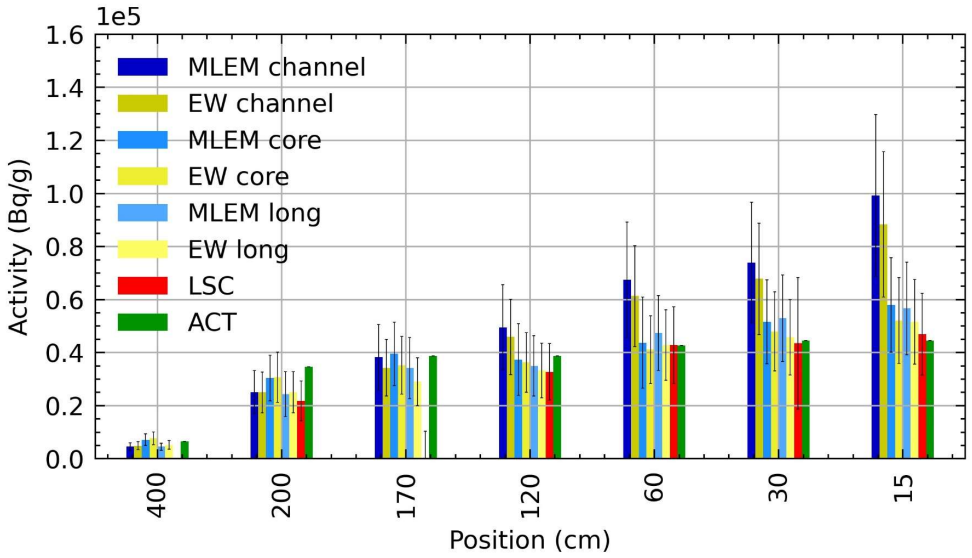

Figure 8: ^{14}C mass activity profile in channel 36-17C. Comparison of results obtained using non-destructive beta spectrometry, liquid scintillation, and neutron activation calculations. MLEM values represent the mean between beta and beta+gamma deconvolution.

V.I. B2 core drill samples

V.I.I. ^{14}C mass activity

We analyzed each face for the graphite brick-sized samples from the B2 drill core by performing an MLEM algorithm deconvolution of the beta+gamma and beta spectrum. Fig. 9 shows the ^{14}C mass activity evaluated by MLEM deconvolution of non-destructive beta spectrometry and neutron activation calculation. Position 0 corresponds to the beginning of the reflector, i.e., the point farthest from the center of the reactor.

The maximum relative deviation between activity estimated by beta+gamma and beta deconvolution is 6%, confirming the findings observed in previous samples. The additional gamma measurement can thus be omitted when measuring larger volume samples (700 cm^3) despite the worst beta-to-gamma signal ratio.

The ^{14}C activation profile along the drill core consistently mirrors the neutron activation calculations within the innermost region of the reactor (>150 cm). This region is characterized by a nearly uniform profile, featuring mass activity values approximately equal to 30000 $Bq.g^{-1}$. The maximum difference between measured and estimated ^{14}C activity is below 30%, consistent with measurement uncertainties.

The gap between measurement and activation calculations increases in the peripheral region, with a maximum of 130% at the 50 cm position. The beta signal to gamma noise ratio in the peripheral region is lower, notably due to the presence of ^{152}Eu produced from europium activation in graphite impurities. Neutron activation gradients for ^{152}Eu and other non-pure beta emitters may be significant within the first 20 cm of a sample. Therefore, the homogeneity assumption in Monte Carlo simulations must be revised to account for the gamma-ray self-attenuation within the sample volume.

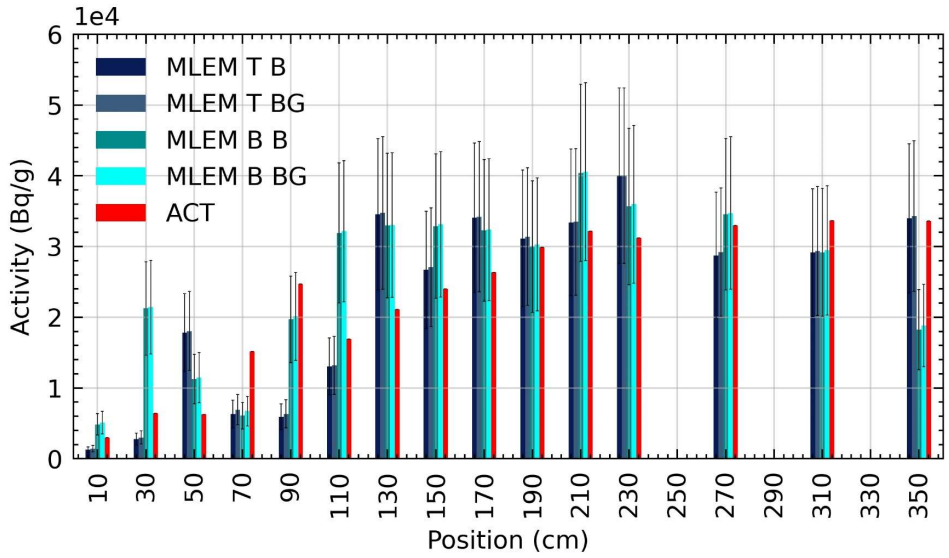

Figure 9: ^{14}C mass activity profile in B2 core drill. Comparison of results obtained using non-destructive beta spectrometry and neutron activation calculations. T = top of the sample, B=bottom of the sample.

Position (cm)	MLEM B (Bq/g)	MLEM BG (Bq/g)	Neutron Activation (Bq/g)
10	$3.1x10^{03}$ (+3%)	$3.3x10^{03}$ (+10%)	$3.0x10^{03}$
30	$1.2x10^{04}$ (+87%)	$1.2x10^{04}$ (+90%)	$6.4x10^{03}$
50	$1.5x10^{04}$ (+132%)	$1.5x10^{04}$ (+136%)	$6.3x10^{03}$
70	$6.2x10^{03}$ (-59%)	$6.8x10^{03}$ (-55%)	$1.5x10^{04}$
90	$1.3x10^{04}$ (-48%)	$1.3x10^{04}$ (-46%)	$2.5x10^{04}$
110	$2.2x10^{04}$ (33%)	$2.3x10^{04}$ (+34%)	$1.7x10^{04}$
130	$3.4x10^{04}$ (60%)	$3.4x10^{04}$ (+61%)	$2.1x10^{04}$
150	$3.0x10^{04}$ (24%)	$3.0x10^{04}$ (+25%)	$2.4x10^{04}$
170	$3.3x10^{04}$ (26%)	$3.3x10^{04}$ (+26%)	$2.6x10^{04}$
190	$3.1x10^{04}$ (2%)	$3.1x10^{04}$ (+3%)	$3.0x10^{04}$
210	$3.7x10^{04}$ (15%)	$3.7x10^{04}$ (+15%)	$3.2x10^{04}$
230	$3.8x10^{04}$ (21%)	$3.8x10^{04}$ (+22%)	$3.1x10^{04}$
270	$3.2x10^{04}$ (-4%)	$3.2x10^{04}$ (-3%)	$3.3x10^{04}$
310	$2.9x10^{04}$ (-13%)	$2.9x10^{04}$ (-13%)	$3.4x10^{04}$
350	$2.6x10^{04}$ (-22%)	$2.7x10^{04}$ (-21%)	$3.4x10^{04}$

Table 3: Comparison of ^{14}C mass activities in ^{14}C for B2 core drill samples. Relative deviation from the activation calculations value in brackets.

V.I.II. Impurities mass activity

Extending the duration of measurements and increasing the sample volume enabled obtaining results on radionuclide activities from impurities in the graphite. Fig. 10 shows the activity distribution for ^{36}Cl, ^{60}Co, ^{90}Sr, ^{133}Ba, ^{137}Cs, ^{152}Eu and ^{154}Eu obtained from MLEM deconvolution of measured spectra.

The average mass activity values fall within the range of $Bq.g^{-1}$, consistent with neutron activation calculations [22]. The obtained results will be compared with alternative measurement methodologies, such as liquid scintillation for pure beta emitters (^{36}Cl and ^{90}Sr) and gamma spectrometry for non-pure beta emitters (^{60}Co, ^{133}Ba, ^{137}Cs, ^{152}Eu, ^{154}Eu). A high-resolution gamma detector would provide additional and more precise information on gamma-emitting radionuclides, improving discrimination between ^{152}Eu and ^{154}Eu. The two radionuclides generate similar responses in the EJ200 plastic scintillator detector (see Fig. 5), thus complicating the analysis of the measured spectra by MLEM. Fig. 11 shows an example of a measured spectrum and its MLEM reconstruction.

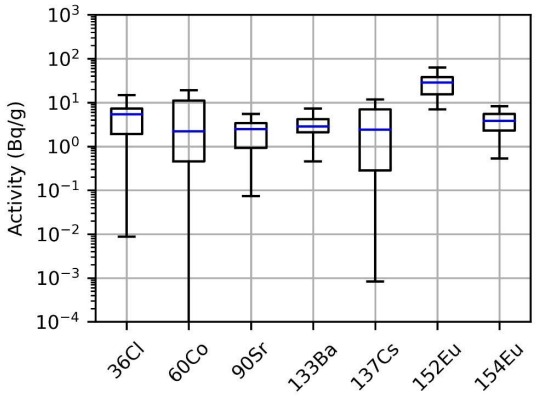

Figure 10: Activity distribution of graphite impurities for B2 core drill samples. The boxes are drawn from the lower quartile (25th percentile) to the upper quartile (75th percentile) with a blue horizontal line to denote the median. Whiskers are based on the 1.5 IQR (Interquantile range) value.

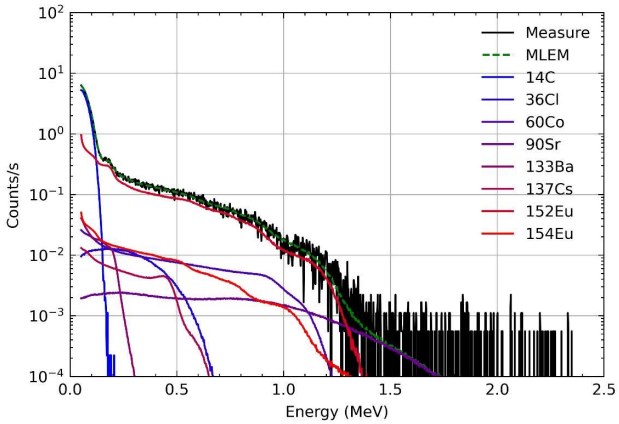

Figure 11: Measured and reconstructed beta+gamma spectrum for the B2 core drill sample at 50 cm from the top of the reactor.

VI: Conclusion

This work showed the relevance of non-destructive beta spectrometry coupled with MLEM deconvolution for the characterization of i-graphite.

Non-destructive beta spectrometry measurements were carried out on samples derived from the fuel channels and vertical drilling of the G1 reactor. MLEM deconvolution of the measured spectra allowed us to estimate the ^{14}C mass activity in the samples. The coherence between the results obtained by deconvolution of the beta+gamma and beta spectra suggests the potential for a simplified mechanical design. This simplification will allow for halving the overall measurement time in future applications.

The results for samples extracted from channel 36-17C exhibited heightened activity on the channel's face compared to the other two faces measured, stemming from the surface reaction $^{14}N(n,p)^{14}C$ or alpha contamination. The mass activities obtained through beta spectrometry exhibit overall consistency, considering the associated uncertainties, compared to values obtained from neutron activation calculations and destructive liquid scintillation.

The results obtained for samples from core drill B2 validated the ^{14}C measurement methodology on larger volume samples. The mass activity values in ^{14}C are consistent with activation calculations in the central region of the core. Analyzing samples collected at the periphery will require a better understanding of the activation distribution along the 20 cm length. Mass activities obtained for other radionuclides

from graphite impurities (^{36}Cl, ^{60}Co, ^{90}Sr, ^{133}Ba, ^{137}Cs, ^{152}Eu, ^{154}Eu) are consistent with activation calculations. Additional measurement techniques like digital autoradiography and high-resolution gamma spectrometry will help refine the findings.

The advantages of the proposed methodology are evident as it is non-destructive, relatively inexpensive and provides automated analysis of measured spectra. The methodology is, therefore, a strong candidate for graphite reactor decommissioning projects. Ongoing studies aim to adapt the methodology for characterizing activated and contaminated graphite and direct *in-situ* application. Additionally, current research explores the application of Artificial Neural Networks (ANNs) for deconvolution, evaluating their potential as an alternative to the MLEM algorithm. The ultimate objective is to develop a technology capable of real-time, *in-situ* characterization of beta-emitting radionuclides.

References

[1] A. V. Bushuev *et al.*, 'Radioactive Contamination of Spent Reactor Graphite', *At. Energy*, vol. 117, no. 3, pp. 196–200, Jan. 2015, doi: 10.1007/s10512-014-9910-4.

[2] 'Wayback Machine'. Accessed: Mar. 26, 2024. [Online]. Available: https://web.archive.org/web/20111016080423/http://nuclear.energy.gov/pdfFiles/DE00782931.pdf

[3] I. Llopart-Babot *et al.*, 'A comparison of different approaches for the analysis of 36Cl in graphite samples', *Appl. Radiat. Isot.*, vol. 202, p. 111046, Dec. 2023, doi: 10.1016/j.apradiso.2023.111046.

[4] V. Remeikis *et al.*, 'Rapid analysis method for the determination of 14C specific activity in irradiated graphite', *PLoS ONE*, vol. 13, no. 1, p. e0191677, Jan. 2018, doi: 10.1371/journal.pone.0191677.

[5] S. Temple, 'Liquid scintillation counting: how has it advanced over the years and what does the future hold?', *Bioanalysis*, vol. 7, no. 5, pp. 503–505, Mar. 2015, doi: 10.4155/bio.15.10.

[6] J. Venara *et al.*, 'Design and development of a portable β-spectrometer for 90Sr activity measurements in contaminated matrices', *Nucl. Instrum. Methods Phys. Res. Sect. Accel. Spectrometers Detect. Assoc. Equip.*, vol. 953, p. 163081, Feb. 2020, doi: 10.1016/j.nima.2019.163081.

[7] A. V. Chesnokov *et al.*, 'A method for measuring in situ a specific soil activity of 90Sr', *Nucl. Instrum. Methods Phys. Res. Sect. Accel. Spectrometers Detect. Assoc. Equip.*, vol. 443, no. 1, pp. 197–200, Mar. 2000, doi: 10.1016/S0168-9002(99)01006-2.

[8] A. Schilk, K. H. Abel, D. Brown, R. Thompson, M. Knopf, and C. Hubbard, 'Selective, high-energy beta scintillation sensor for real-time, in situ characterization of uranium-238 and strontium-90', 1995, doi: 10.1007/BF02041923.

[9] B.-K. Seo, C.-H. Park, K.-W. Lee, dong-gyu Lee, and C.-H. Jung, 'Development of the In-situ Monitoring System for Pipe Internal Contamination Measurement in the Decommissioning Site', *J. Nucl. Sci. Technol.*, vol. 45, pp. 500–502, Aug. 2014, doi: 10.1080/00223131.2008.10875900.

[10] P. Fichet, F. Bresson, A. Leskinen, F. Goutelard, J. Ikonen, and M. Siitari-Kauppi, 'Tritium analysis in building dismantling process using digital autoradiography', *J. Radioanal. Nucl. Chem.*, vol. 291, no. 3, pp. 869–875, Mar. 2012, doi: 10.1007/s10967-011-1423-1.

[11] G. Laurent *et al.*, 'New concepts and instruments for 14C and 36Cl measurements in i-graphite'.

[12] N. Dufour, A. Sari, G. H. V. Bertrand, and F. Carrel, 'Scintillating fibre based beta spectrometer: Proof of concept by Monte-Carlo simulation and first experimental assessment', *Nucl. Instrum. Methods Phys. Res. Sect. Accel. Spectrometers Detect. Assoc. Equip.*, vol. 1010, p. 165548, Sep. 2021, doi: 10.1016/j.nima.2021.165548.

[13] R. Remetti and A. Sessa, 'Beta spectra deconvolution for liquid scintillation counting', *J. Radioanal. Nucl. Chem.*, vol. 287, no. 1, pp. 107–111, Jan. 2011, doi: 10.1007/s10967-010-0882-0.

[14] S. Joung *et al.*, 'Simultaneous quantitative analysis of 3H and 14C radionuclides in aqueous samples via artificial neural network with a liquid scintillation counter', *Appl. Radiat. Isot.*, vol. 170, p. 109593, Apr. 2021, doi: 10.1016/j.apradiso.2021.109593.

[15] K. Yamada, Y. Takeuchi, G. Igarashi, and M. Osako, 'Field Survey of Radioactive Cesium Contamination in Concrete After the Fukushima-Daiichi Nuclear Power Station Accident', *J. Adv. Concr. Technol.*, vol. 17, no. 12, pp. 659–672, Dec. 2019, doi: 10.3151/jact.17.659.

[16] L. A. Shepp and Y. Vardi, 'Maximum Likelihood Reconstruction for Emission Tomography', *IEEE Trans. Med. Imaging*, vol. 1, no. 2, pp. 113–122, 1982, doi: 10.1109/TMI.1982.4307558.

[17] J. Venara, 'Méthode et dispositif pour la caractérisation radiologique non destructive du 14C dans les graphites activés sous flux neutronique', FR2214724

[18] F. Goutelard *et al.*, 'Investigation Program of the G1 Reactor: Towards Better Knowledge to Prepare Dismantling Operations', p. 15, Mar. 2023.
[19] Z. Laili, 'Genie TM 2000 spectroscopy software operations, Canberra 52 (1) (2016) 1–361.', 2016.
[20] C. L. Lawson and R. J. Hanson, *Solving Least Squares Problems*. in Classics in Applied Mathematics. Society for Industrial and Applied Mathematics, 1995. doi: 10.1137/1.9781611971217.
[21] L. Fleres *et al.*, 'Design of a reliable numerical model of a plastic scintillation detector for beta spectrometry', *EPJ Web Conf.*, vol. 288, p. 10010, 2023, doi: 10.1051/epjconf/202328810010.
[22] A. Van Lauwe, 'Calcul d'activation du graphite du réacteur G1, DEN/DANS/DM2S/SERMA/LPEC/NT/17-62192/A, CEA Technical report'.
[23] A. J. M. Plompen *et al.*, 'The joint evaluated fission and fusion nuclear data library, JEFF-3.3', *Eur. Phys. J. A*, vol. 56, no. 7, p. 181, Jul. 2020, doi: 10.1140/epja/s10050-020-00141-9.
[24] X. Mougeot, 'BetaShape: A new code for improved analytical calculations of beta spectra', *EPJ Web Conf.*, vol. 146, p. 12015, 2017, doi: 10.1051/epjconf/201714612015.
[25] 'EJ-200, EJ-204, EJ-208, EJ-212 - Plastic Scintillators - Eljen Technology'. Accessed: Jun. 24, 2022. [Online]. Available: https://eljentechnology.com/products/plastic-scintillators/ej-200-ej-204-ej-208-ej-212